

# Assembly of 2D MXene Nanosheets and TiO<sub>2</sub> Nanoparticles for Fabricating Mesoporous TiO<sub>2</sub>@MXene Membranes

*Zhi Xu<sup>1</sup>, Yuqing Sun<sup>2</sup>, Yongxiang Zhuang<sup>2</sup>, Wenheng Jing<sup>2</sup>, Hua Ye<sup>1</sup>, Zhanfeng Cui<sup>1,\*</sup>*

<sup>1</sup>CRMI Technology Centre, Institute of Biomedical Engineering, Department of Engineering Science, University of Oxford, Oxford, UK.

<sup>2</sup>State Key Laboratory of Materials-Oriented Chemical Engineering, College of Chemical Engineering, Nanjing Tech University, 5 Xinmofan Road, Nanjing 210009, PR China.

\*Corresponding author: [zhanfeng.cui@eng.ox.ac.uk](mailto:zhanfeng.cui@eng.ox.ac.uk) (Prof. Z. Cui)

## Abstract

A simple and scalable method was proposed for the preparation of the mesoporous membranes by assembling 2D MXene nanosheets and TiO<sub>2</sub> nanoparticles (NPs) on a macroporous support. MXene nanosheets were introduced into TiO<sub>2</sub> hydrosol, and then transformed the gel for fabrication of mesoporous TiO<sub>2</sub>@MXene membranes. Characterization results confirmed that an assembled structure of TiO<sub>2</sub>@MXene nanosheets was formed, benefiting from the nanosheets as ‘floor tiles’, thereby successfully inhibiting the sol infiltration into the porous support. As a result, the hydrosols could be directly coated on macroporous substrates including a disc support with an average pore size of ~100 nm and a four-channel hollow fiber with an average pore size of ~300 nm. It should be emphasized that the integrated disc or hollow fiber TiO<sub>2</sub>@MXene membranes were fabricated by only one single cycle of coating, aging and calcination. A range of advanced membrane characterization techniques were employed to study the ultrastructure of the fabricated membranes and the assumption of introducing nanosheets to prevent membrane defect and gel infiltration was validated. Filtration experiments revealed the resulted membranes, in particular the hollow fiber TiO<sub>2</sub>@MXene membranes, had a narrow pore size distribution, desirable rejection characteristics and high permeate flux. The 2D nanosheet assisted TiO<sub>2</sub> NPs assembly proposed in this work promises a simple, feasible and scalable approach for fabrication of high-performance mesoporous TiO<sub>2</sub> membranes.

## 1. Introduction

TiO<sub>2</sub> mesoporous membranes with pore size range of 2~10 nm have been widely studied and utilized in various fields<sup>[1-5]</sup>, including energy storage, food, pharmaceutical and water purification for its high thermal and chemical stability, as well as its high flux and low cost. The sol-gel method<sup>[6-9]</sup> including polymeric route and hydrosol route has been considered as extremely practical for fabricating these membranes, and the hydrosol route is industrially preferred due to its easy-operation, non-toxicity and low-volatilization<sup>[10]</sup>. To obtain a high permeate flux and mechanical strength, the sols are coated on macroporous substrates to obtain supported (composite) mesoporous membranes. In this case, the sol infiltration and membrane cracking are inevitable occurred due to the involved capillary force from the porous substrate. Introduction of nanoparticles to decrease the sol infiltration<sup>[11-12]</sup> and toughen the gels<sup>[8]</sup> have been proposed in our previous work, however, repetitious coating and sintering resulted in a long producing cycle and high cost. Alternatively, introducing two-dimensional nanosheets into the sols to inhibit the sol infiltration might be a better choice than the nanoparticles.

As a kind of novel membrane material, two-dimensional (2D) materials, such as graphene and graphene oxide (GO),<sup>[13-15]</sup> metal-organic frameworks (MOFs) nanosheets<sup>[16]</sup>, zeolite nanosheets,<sup>[17]</sup> and molybdenum disulfide have been reported for fabrication of membranes<sup>[18]</sup>. Recently, a novel kind of 2D layered material named MXene, a family of transition metal carbides, has been exploited and developed.<sup>[19]</sup> The most studied MXene has been Ti<sub>3</sub>C<sub>2</sub>T<sub>x</sub>, which was delaminated successfully in 2011<sup>[20]</sup> and widely used in super capacitors,<sup>[21]</sup> lithium-ion batteries<sup>[22]</sup>, oxygen evolution reaction<sup>[23]</sup> and heavy metal adsorption.<sup>[24, 25]</sup> On the one hand, a few reports has demonstrated that MXene materials can be fabricated as membranes showing great potential for water purification<sup>[26, 27]</sup>. On the other hand, the precise control of the interlayer spacing of the laminar 2D-material membranes, which has been realized for GO membranes in our recent work<sup>[28]</sup>, while remains challenge for MXene membranes for now. This might limit the MXene membranes for

efficient ions sieving. Alternatively, the integration of 2D nanosheets with 3D nanocrystals has been considered as another promising approach to develop high-performance separation membranes<sup>[29-31]</sup>.

Herein, we propose a novel approach to fabricate  $\text{TiO}_2$  mesoporous membranes by assembling 2D  $\text{Ti}_3\text{C}_2\text{T}_x$  MXene nanosheets and  $\text{TiO}_2$  nanoparticles to enable directly coating the aqueous sols on a macroporous substrate. As shown in Figure 1, the MXene nanosheets provide 2D platforms for depositing  $\text{TiO}_2$  nanoparticles, thereby preventing the penetration of  $\text{TiO}_2$  nanoparticles into the macropores of ceramic support during the sol coating process. Meanwhile, the MXene nanosheets with micrometer lateral size would seal the potential macroporous defects on the ceramic support thereby reducing the dependence of the mesoporous membrane performance on the macroporous substrate. Disc membranes and hollow fiber membranes are fabricated by spin-coating and dip-coating, respectively and their nanostructures and filtration performance are investigated in detail.

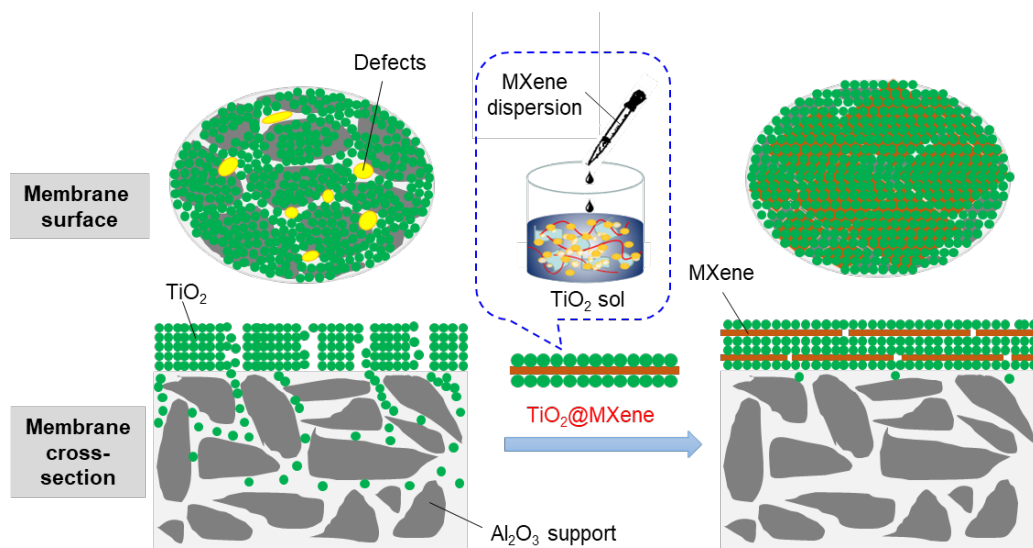


**Figure 1.** Fabrication of  $\text{TiO}_2$ @MXene membranes to eliminate potential defects

## 2. Experimental

### 2.1 Materials and membrane supports

TiO<sub>2</sub> nanoparticles with a particle size of 5 nm (P5) were purchased from Xuan Cheng Jing Rui New Materials Co., Ltd (China). The additives selected in this work were polyvinyl alcohol (PVA, Sigma–Aldrich, MW=61,000Da) and hydroxyethyl cellulose (HEC, Sigma–Aldrich, MW=90,000Da). Ti<sub>3</sub>AlC<sub>2</sub> particles and HF (analytical grade) were purchased from Sinopharm Chemical Reagent Co., Ltd. (China). In all experiments deionized (DI) water was used.  $\alpha$ -Al<sub>2</sub>O<sub>3</sub> particles (particle size of 500 nm) were supplied by Jiangsu Jiuwu Hi-Tech Ltd (China). Paraffin was purchased from Sinopharm Chemical Reagent Co., Ltd. (China).

To fabricate flat sheet membranes, an alumina support with a macroporous structure was first prepared. An alumina powder with an average size of 0.5  $\mu$ m was mixed with poly(vinyl alcohol) (PVA) and paraffin and then pressed at 10 MPa for 60 s. The pressed disks were finally sintered at 1200 °C with the heating and cooling rates of 2 °C/min for 2 hours to get robust supports. The diameter, thickness, and pore size of the alumina supports were 28.5 mm, 2.2 mm, and 0.1  $\mu$ m, respectively. The pore size distribution of the support is shown in Figure 2(a).

The four-channel  $\alpha$ -Al<sub>2</sub>O<sub>3</sub> hollow fiber module supports were supplied by Jiangsu Jiutian Hi-Tech Ltd (China). These supports ( $d_i$ =1 mm,  $d_o$ =4 mm) with an average pore diameter of 300 nm and a high pure water flux of 2200 L/(m<sup>2</sup>•h•bar) used in this study were fabricated by the phase inversion-sintering method based on a dry/wet spinning process.<sup>[32]</sup> Further details on the production process of the membranes was given by Gu et al.<sup>[33]</sup>. The pore size distribution of these supports is shown in Figure 2(b).

## 2.2 Synthesis of MXene nanosheets.

Ti<sub>3</sub>AlC<sub>2</sub> particles were first etched by HF solution to generate Ti<sub>3</sub>C<sub>2</sub>T<sub>x</sub> nanosheets. By extracting Al as AlF<sub>3</sub>, the interaction between the layers is weakened. The MXene nanosheets can be obtained by sonication-assisted exfoliation. Typically, the resulting Ti<sub>3</sub>C<sub>2</sub>T<sub>x</sub> powders were dispersed in DI water with concentration of 2 mg/mL. To delaminate Ti<sub>3</sub>C<sub>2</sub>T<sub>x</sub>, the solution was sonicated for 1 h under flowing argon

and then centrifugation for 1 h at 3500 r.p.m (TGL-16G, Shanghai, China). The supernatant including stable  $\text{Ti}_3\text{C}_2\text{T}_x$  nanosheets was collected into glass bottle.

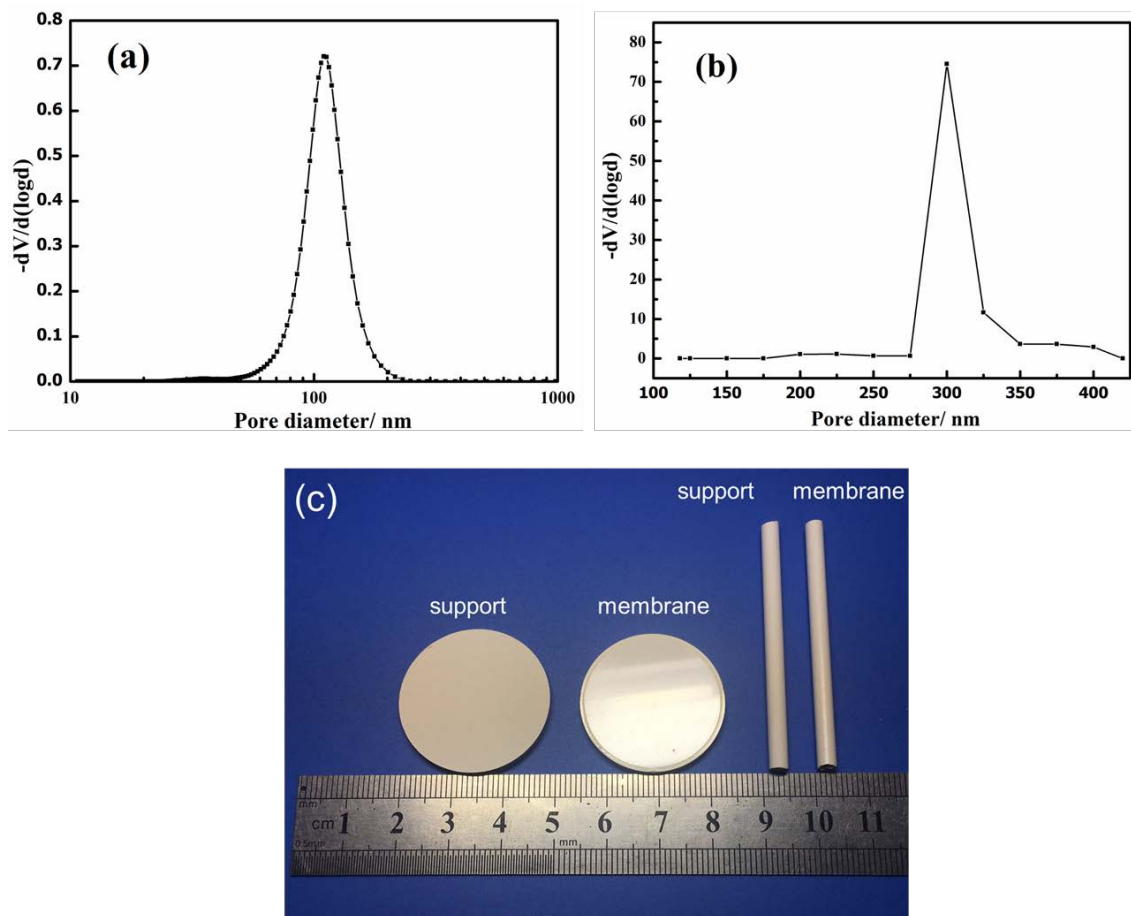


**Figure 2.** Pore size distribution of supports: (a)  $\alpha\text{-Al}_2\text{O}_3$  disc; (b) four-channel  $\alpha\text{-Al}_2\text{O}_3$  hollow fiber; and (c) photos of support and membrane of disc and 4-channel hollow fiber

### 2.3 Synthesis of $\text{TiO}_2@\text{MXene}$ membranes.

A Titania hydrosol used in this study was prepared as follows: 0.6 g P5 was added into 30 mL of deionized water and dispersed by stirring followed by ultrasonic dispersion for 2 min at 250 W (SK5210HP, Shanghai, China). Then,  $\text{Ti}_3\text{C}_2\text{T}_x$  (1.6mg/L) was dissolved in the above dispersions at varying concentration (0, 0.5 wt%, and 1 wt%) and stirred for 15min to obtain homogenous solutions. Then, 20 mL of HEC (3 wt%)

solution and 10 mL of PVA (0.5 wt%) solution were added dropwise to the above solutions to obtain the final sol and HEC also acted as a drying control chemical additive.

The flat sheet membrane is fabricated by spin-coating of the prepared sol on the disc ceramic substrate at 3000 rpm for 30 s. The coated films were dried and aged for 12 h at 60 °C in an oven and then calcined in air at 400 °C with a heating and cooling rate of 0.5 °C/min to obtain a mesoporous membrane. TiO<sub>2</sub>@MXene hollow fiber membranes were prepared by dip-coating the above coating sols on the outer surface of the four-channel  $\alpha$ -Al<sub>2</sub>O<sub>3</sub> hollow fiber support with a pre-determined coating time of 30 s, withdraw speed of 1 cm/s, and repeating 4 times. The sol coated hollow fiber was dried, aged, and calcinated in air at 400 °C for 4 h with a heating and cooling rate of 0.5 °C/min. The support and resulted membrane samples are shown in Figure 2(c).

## 2.4 Characterization

The surface morphology and thickness of the membrane were observed by a field-emission scanning electron microscopy (FE-SEM, Hitachi S4800). For the same sample for FE-SEM, the scanning of spectrum of energy dispersion of X-ray (EDX) was used to investigate the element distribution on the surface and cross section of the composite membrane. The AFM measurements were performed by using an XE-100 atomic force microscope. XRD measurements (Bruker D8 Advance X-ray diffractometer with Cu K $\alpha$  radiation with  $\lambda$  of 0.154 nm at 40 kV and 30 mA) were used for the determination of the phase composition and the average size of the membrane material. X-ray photoelectron spectroscopy (XPS) data were collected on an AXIS-Ultra instrument using monochromatic Al K $\alpha$  radiation (225W, 15mA, 15kV). The membrane permeability was determined by the permeation measurement using deionized water. The rejection characteristics of the membranes was evaluated by measuring 3g/L dextran solution with four different molecular weights of 10,000, 40,000, 70,000 and 500,000 Da, according to the ASTM E1343-90 method. The molecular weight of the 90% retained dextran was taken as the MWCO of the membrane. The concentrations and molecular weights of dextran in the feed and permeate solutions were analyzed by gel permeation chromatography (Waters Co., Milford, MA). Raman spectra were collected through a Renishaw 2000 model

confocal microscopy Raman spectrometer with a CCD detector and a holographic notch filter (Renishaw Ltd., Gloucestershire, U.K.) at ambient conditions, using the radiation of 514.5 nm from an air-cooled argon ion laser to excite the SERS. Particle size and size distribution of prepared sols were measured by the phase analysis light scattering technique (ZetaPALS, Brookhaven, USA).

### 3. Results and Discussion

#### 3.1 Hydrosols of TiO<sub>2</sub>@MXene

The MXene nanosheets were characterized by SEM and AFM, and the images are shown in Figure 3. The lateral size is approximately 500 nm with a thickness of 1~2 nm, indicating a single- or double-layered structure of MXene<sup>[34]</sup>. This 2D MXene nanosheets would be desirable for the deposition of TiO<sub>2</sub> NPs, and meanwhile inhibiting the infiltration of TiO<sub>2</sub> NPs into the pores of the ceramic support, which will be discussed later.

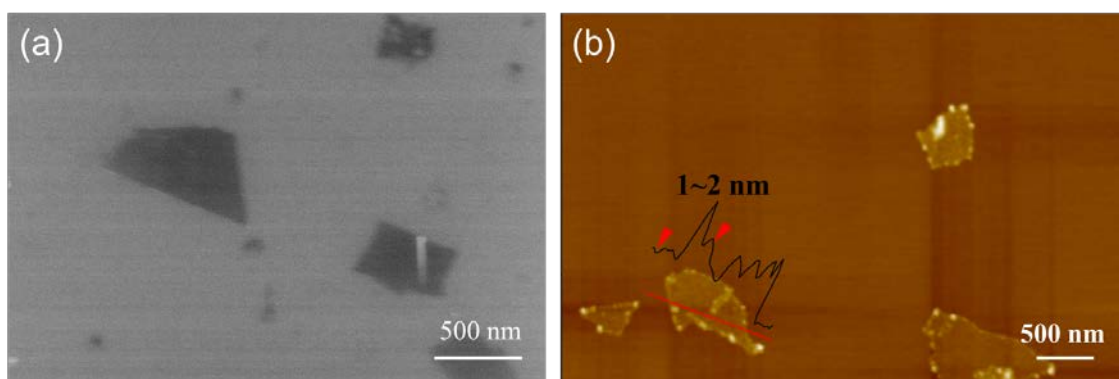


**Figure 3.** (a) SEM and (b) AFM image of MXene nanosheets

For the formation of an integrated, crack-free TiO<sub>2</sub> mesoporous membrane, sols with a small and uniform particle size were required. The stable hydrosols of TiO<sub>2</sub>@MXene were prepared by ultrasonic assistance, as evidenced by the photos shown in Figure 4 (a). Furthermore, the particle size distribution of the sols with 2D MXene of 0, 0.5 wt%, 1 wt% was characterized by DLS and the results are shown in Figure 4 (b). It is found that the sols present narrow monomial distributions with an average particle size of 15 nm,

suggesting that the introduction of 2D MXene nanosheets did not affect the particle size of the pristine  $\text{TiO}_2$  hydrosols.

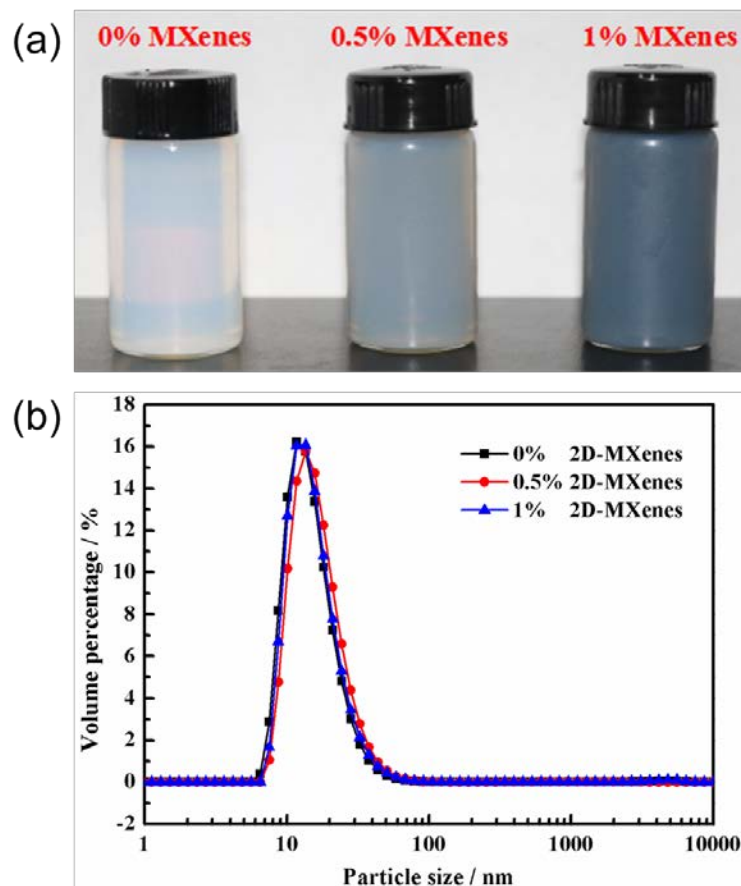


**Figure 4.** (a) Photographs and (b) particle size distribution of the  $\text{TiO}_2$  hydrosol with different mass fraction of MXene

Furthermore, TEM were performed to observe the morphology and the dispersibility of the pristine  $\text{TiO}_2$  and  $\text{TiO}_2$ @MXene hydrosols. As shown in Figure 5 (a-b),  $\text{TiO}_2$  NPs with single particle size of 5 nm were uniformly dispersed in the pristine sol. The comparison with DLS result of 15 nm particle size distribution suggests that a few  $\text{TiO}_2$  NPs aggregated in the sol due to the intrinsically attractive forces between  $\text{TiO}_2$  NPs, which however would not affect the coating process. By adding 1 wt% of these MXene nanosheets in the  $\text{TiO}_2$  sol, the  $\text{TiO}_2$  NPs were homogeneously deposited on the 2D MXene nanosheets, without any morphology changes in both MXene and  $\text{TiO}_2$  NPs, as displayed in Figure 5 (c-d).



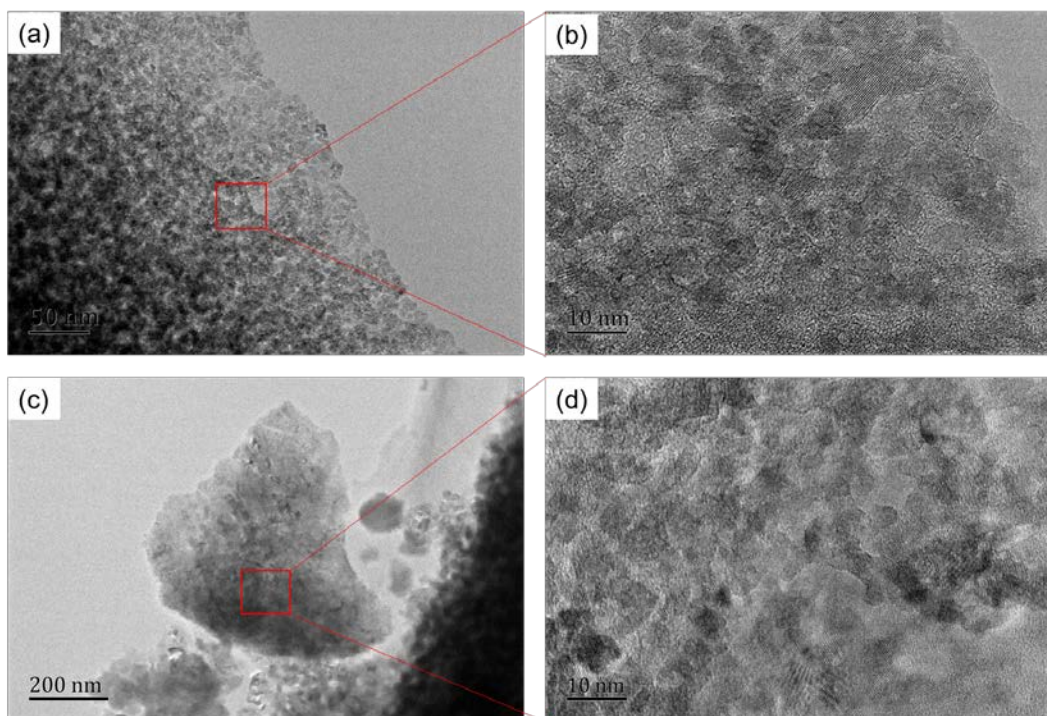


**Figure 5.** TEM images of the hydrosol of (a, b)  $\text{TiO}_2$  and (c, d)  $\text{TiO}_2@\text{MXene}$  (1 wt%).

Sufficient thermal stability is another precondition for fabricating the  $\text{TiO}_2$ -based mesoporous membranes since the sol layer coated on the support must undergo a calcination process at high temperature to form an integrated separation layer. Thus, we studied the thermal properties of the  $\text{TiO}_2@\text{MXene}$  sol by using the calcination protocol for fabricating pristine  $\text{TiO}_2$  membranes. As shown in Figure 6, incorporating the robust MXene improves the thermal stability of the sol, indicated by the higher decomposition temperature of the  $\text{TiO}_2@\text{MXene}$  (1 wt%) than the pristine  $\text{TiO}_2$  sol. This result ensures the successful calcination of the  $\text{TiO}_2@\text{MXene}$  sol into membrane by following the same protocol for the pristine  $\text{TiO}_2$  membranes.

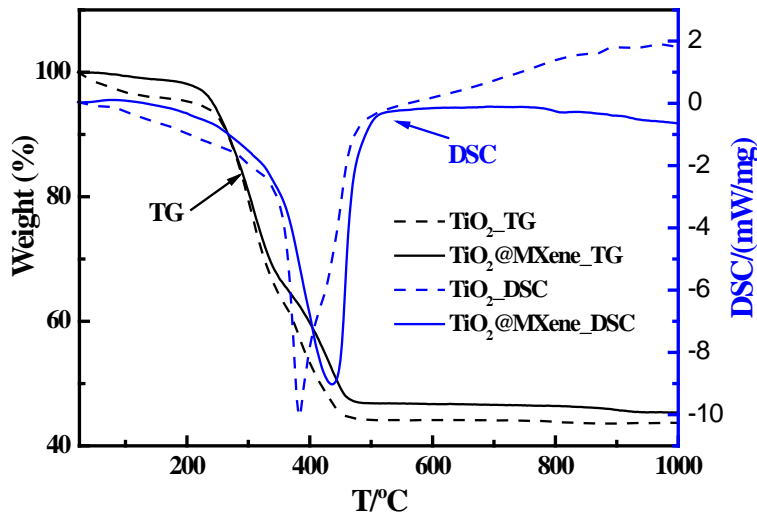


**Figure 6.** TGA curves of TiO<sub>2</sub> sol and TiO<sub>2</sub>@MXene (1 wt%) sol

Raman spectroscopy was used to further study the structure of TiO<sub>2</sub> and TiO<sub>2</sub>@MXene with MXene fraction of 1 wt%, as shown in curves a and b in Figure 7, respectively. In the pristine TiO<sub>2</sub> spectrum (curve a), there are a strong peak at 144 cm<sup>-1</sup>, together with three other peaks at 394, 513, and 635 cm<sup>-1</sup>, which could be assigned to the anatase vibrational modes. In the TiO<sub>2</sub>@MXene samples (curve b), besides of the above peaks for pristine TiO<sub>2</sub>, the two broad peaks between 1000 and 1800 cm<sup>-1</sup> were characteristic for the D- and G- modes of graphitic carbon.

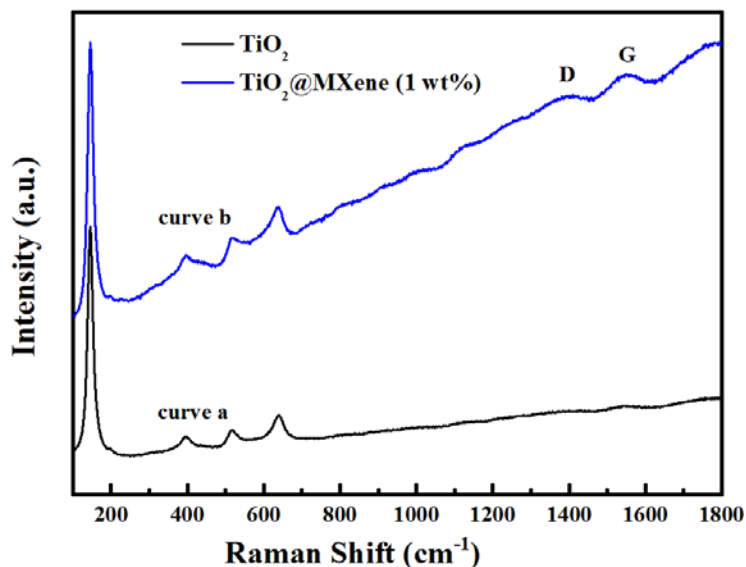


**Figure 7.** Raman spectra of TiO<sub>2</sub> and TiO<sub>2</sub>@MXene (1 wt%)

XPS spectra of  $\text{TiO}_2$  and  $\text{TiO}_2\text{@MXene}$  (1 wt%) were recorded to study the chemical properties, as shown in Figure 8. In general, the full scan spectrum clearly shows the F element in the 1% MXene- $\text{TiO}_2$  sample, which is corresponding to one of the specific elements of MXene nanosheets resulting from the LiF etching process. Meanwhile, from the O1s spectra, a new peak at around 530.5 eV, corresponding to the hydroxyl groups of MXene nanosheet, is also found in the MXene- $\text{TiO}_2$  sample, again confirming the present of MXene in the  $\text{TiO}_2$ <sup>[35]</sup>. In addition, the peak related to the C=O group of  $\text{TiO}_2$  was shifted from 531 eV to 532 eV, and the peak related to the O-Ti/OH group of MXene was shifted from 531.7 eV to 530.5 eV in the MXene- $\text{TiO}_2$  sample. It might suggest favorable interactions between MXene and  $\text{TiO}_2$ , which would promote the deposition of  $\text{TiO}_2$  NPs on the MXene nanosheet.

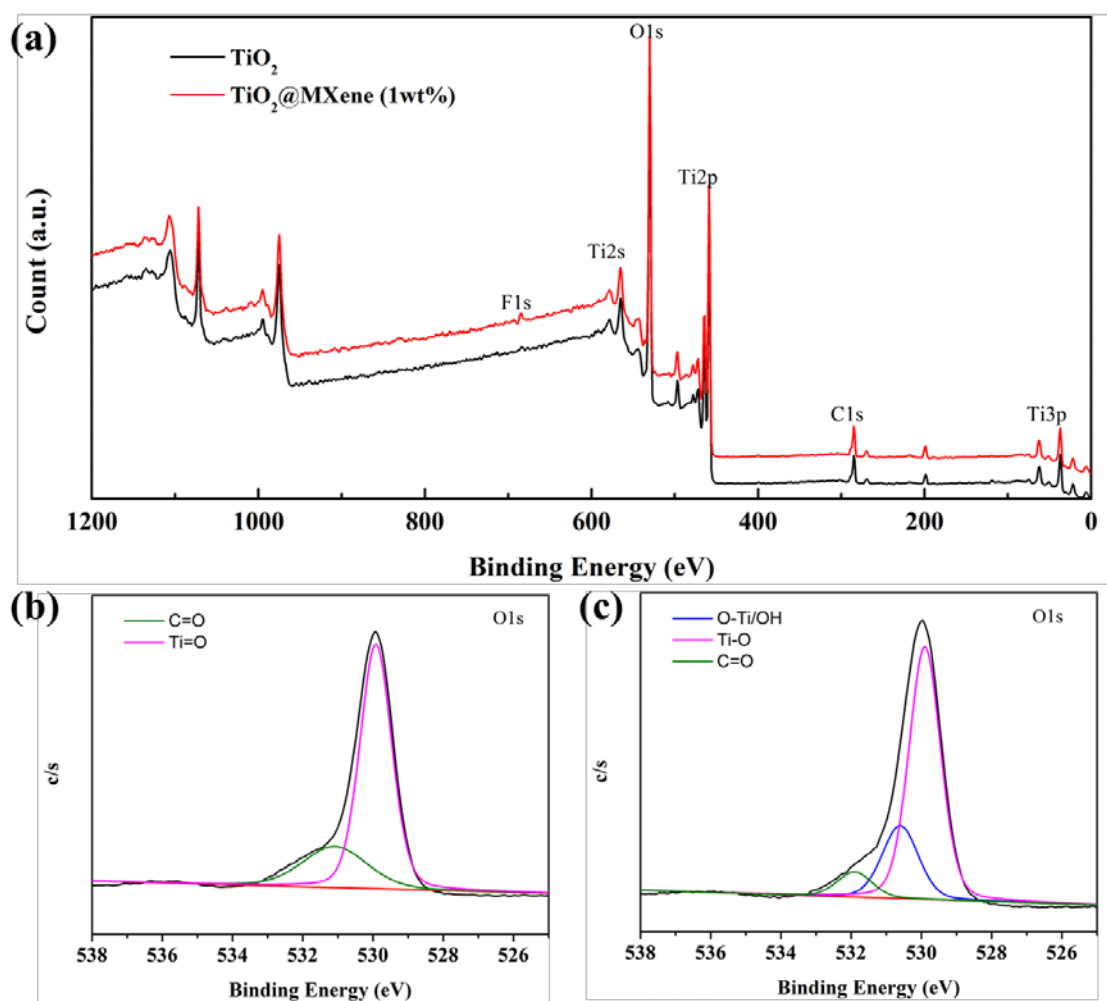


**Figure 8.** XPS spectra of the  $\text{TiO}_2$  and  $\text{TiO}_2$  with 1 wt% of MXene: (a) full scan; (b) O1s of  $\text{TiO}_2$  and (c) O1s of  $\text{TiO}_2$  with 1 wt% of MXene.

### 3.2 TiO<sub>2</sub>@MXene disc membranes.

To obtain a supported mesoporous membrane, the TiO<sub>2</sub> hydrosols with different mass fraction of MXene were spin-coated on a macroporous Al<sub>2</sub>O<sub>3</sub> disc, following by drying and calcination. SEM observations were carried out to study the surface and cross-section morphology of the resulting membranes as shown in Figure 9. Distinct porous structures can be observed in the disc support, providing highly reduced transport resistance for the mesoporous composite membrane. No cracks can be found in the membrane surface after depositing the separation layer on the porous ceramic disc (Figures 9 a&d), indicating integrated mesoporous membranes were fabricated successfully. However, some dents caused by sol infiltration emerged on the surface of the membrane fabricated by pristine TiO<sub>2</sub> NPs hydrosol. It is observed the number of dents was decreased with the increase of MXene contents in the TiO<sub>2</sub>@MXene hydrosol, and the membrane with the smoothest surface is achieved by adding amount of 1 wt% MXene. In the cross-sections shown in Figures 9 (e-f), the sol infiltration is significant in the pristine TiO<sub>2</sub> membrane (Figure 9f) which would result in the possible defects in the separation layer to decrease the selectivity, as well as high transport resistance to lower the permeate flux. In comparison, by introducing the 2D MXene nanosheets, the sol infiltration was inhibited significantly. No infiltration is observed in the TiO<sub>2</sub>@MXene membrane with 1% MXene (Figure 9h). As a result, an integrated separation layer with a thickness of  $\sim 2\ \mu\text{m}$  was formed in the TiO<sub>2</sub>@MXene composite membranes.

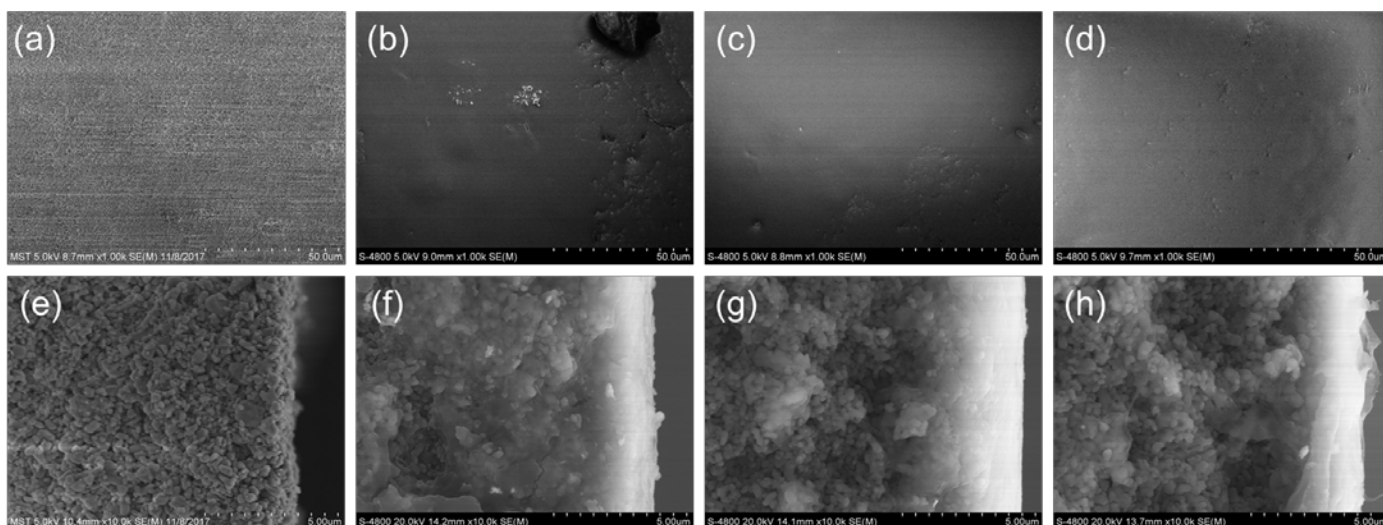


**Figure 9.** SEM images of the surface (a-d) and cross section (e-h) of the (a, e) disc support; (b, f)  $\text{TiO}_2$  membrane; (c, g)  $\text{TiO}_2$ @MXene (0.5 wt%) membrane; (d, h)  $\text{TiO}_2$ @MXene (1 wt%) membrane.

AFM was used to further study the ultra nanostructures of the  $\text{TiO}_2$  membrane surface before and after introducing MXene nanosheets, and the results are shown in Figure 10. Compared with the pristine  $\text{TiO}_2$  membrane, the surface of the MXene nanosheets incorporated  $\text{TiO}_2$  membrane exhibits more uniform morphologies. By analyzing the surface roughness, we found that the surface roughness ( $R_a$  and  $R_q$  are the arithmetic average of the absolute values and the root mean square average of height deviation taken from the mean image data plane, respectively) of the  $\text{TiO}_2$  membrane was gradually decreased by increasing the MXene amount in the membrane. This result suggests that the aid of MXene nanosheets could regulate the assembly of  $\text{TiO}_2$  NPs and lead a more uniform and integrated membrane surface.

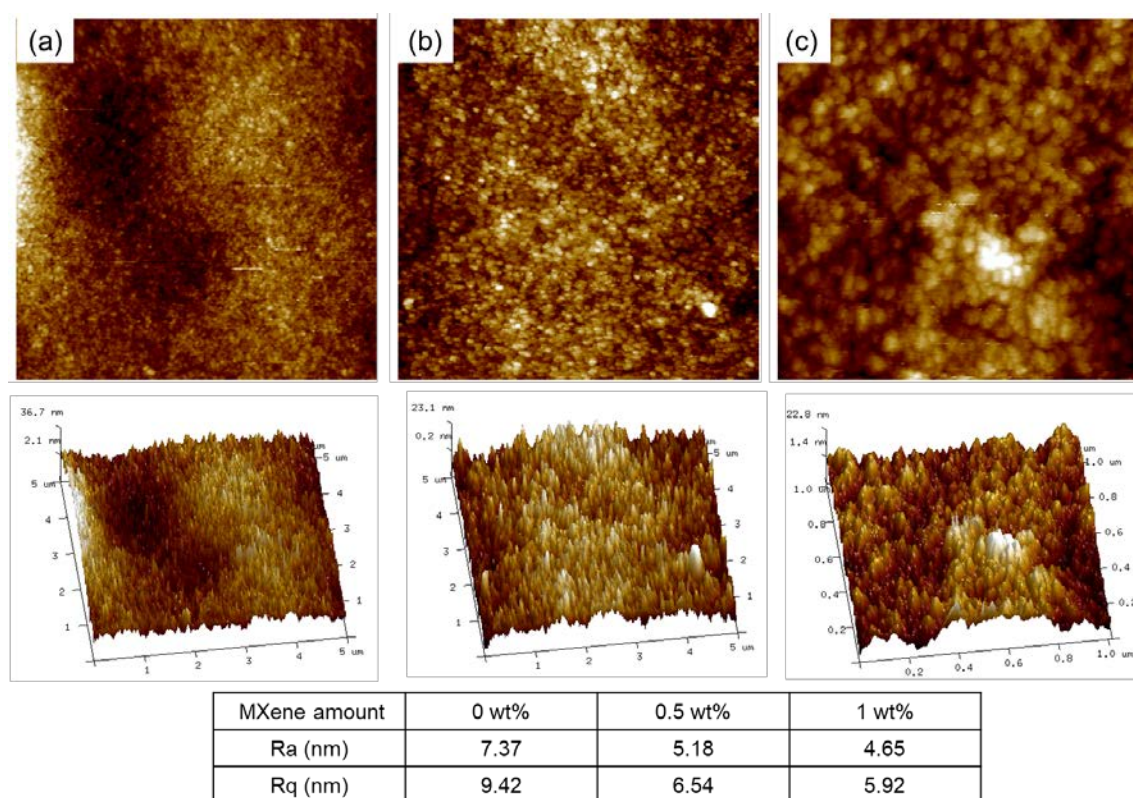


**Figure 10.** AFM images of the surface of the TiO<sub>2</sub> mesoporous membranes with different MXene content. (a) 0%; (b) 0.5 wt%; and (c) 1 wt%, with average surface roughness listed in the table.

The permeability of the fabricated membranes and the effect of the mass fraction of MXene in the TiO<sub>2</sub> disc membranes were shown in Figure 11 (a). The water flux of the support is determined to be 13.4 L m<sup>2</sup> h<sup>-1</sup> bar<sup>-1</sup>, and the flux decreased after coating the TiO<sub>2</sub>-based separation layer. Introduction of MXene nanosheets also slightly reduces the flux of pristine TiO<sub>2</sub> membrane, which can be attributed to the improved integration of the separation layer as indicated by the SEM results (Figure 9). By increasing the MXene loading in the membrane from 0.5 to 1 wt%, the water flux can be increased from 8.9 to 9.9 L m<sup>2</sup> h<sup>-1</sup> bar<sup>-1</sup>, suggesting the enhanced prevent of sol infiltration with the aid of 2D MXene nanosheets in the hydrosol.

Figure 11(b) shows the measured rejection characteristics. As seen in the figure, the much improved retention was achieved by introducing MXene nanosheets. The poor retention in the pristine TiO<sub>2</sub> membrane suggests the existence of macroporous defects in the separation layer. By contrast, 90% molecular weight cutoff (MWCO) of the TiO<sub>2</sub>@MXene membranes with 0.5 wt% and 1 wt% MXene are 50060 and 548900 Da, respectively. The corresponding pore size are 9.6 and 10.0 nm calculated by the classic model  $r = 0.033M^{0.46}$



(nm)<sup>[23]</sup>, promising typical mesoporous membrane structures. It should be pointed out a sharper MWCO curve is required for practical separation applications, indicating further improvements are required.

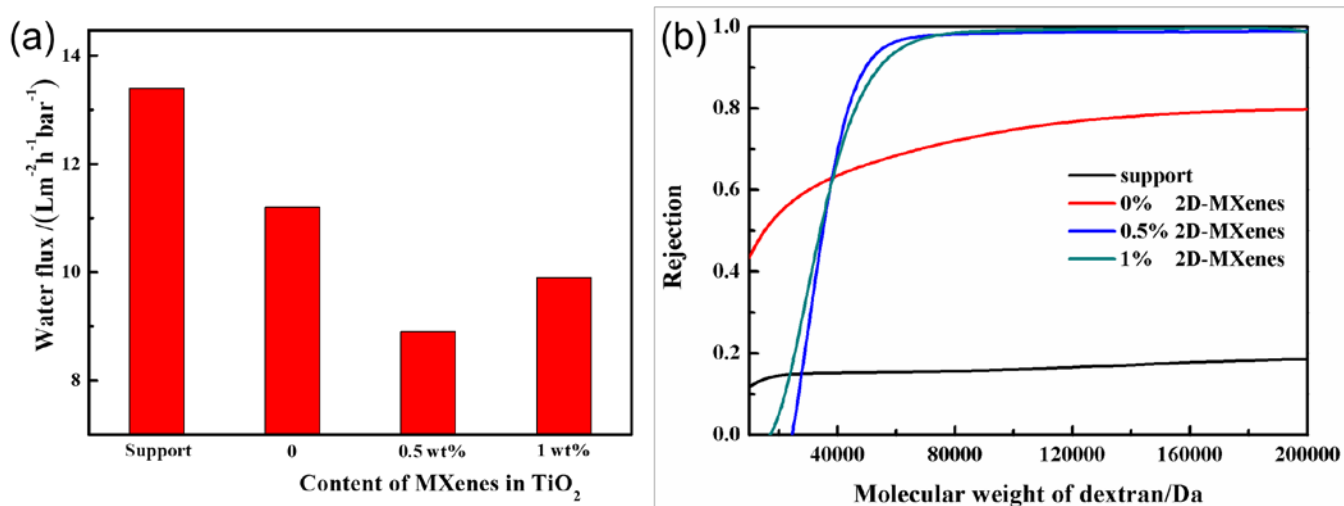


**Figure 11.** Filtration performance of disc membrane: (a) Pure water flux, and (b) dextran rejection of the support, TiO<sub>2</sub> membrane and TiO<sub>2</sub>@MXene membranes with 0.5 or 1 wt% MXene.

### 3.3 TiO<sub>2</sub>@MXene hollow fiber membranes.

To further demonstrate the potential of this feasible TiO<sub>2</sub>@MXene approach for fabricating mesoporous membrane, we also tested with industrially preferred hollow fibers as the support. The hydrosols are deposited on the hollow fiber support via a facile dip-coating method. Specifically, 4-channel  $\alpha$ -Al<sub>2</sub>O<sub>3</sub> hollow fiber supports with average pore size of ~300 nm are fabricated by a spinning phase-inversion method, which produce an asymmetric microstructure consisting of finger-like voids and sponge-like region. Compared with the particle piled pores of the above disc support, the finger-like voids offer much lower transport resistance while more run-through-macropores are also emerged on the support surface (Figures 12 a&d). Thus the sols infiltration might be more serious when the hollow fiber is used for fabrication of the mesoporous membranes.

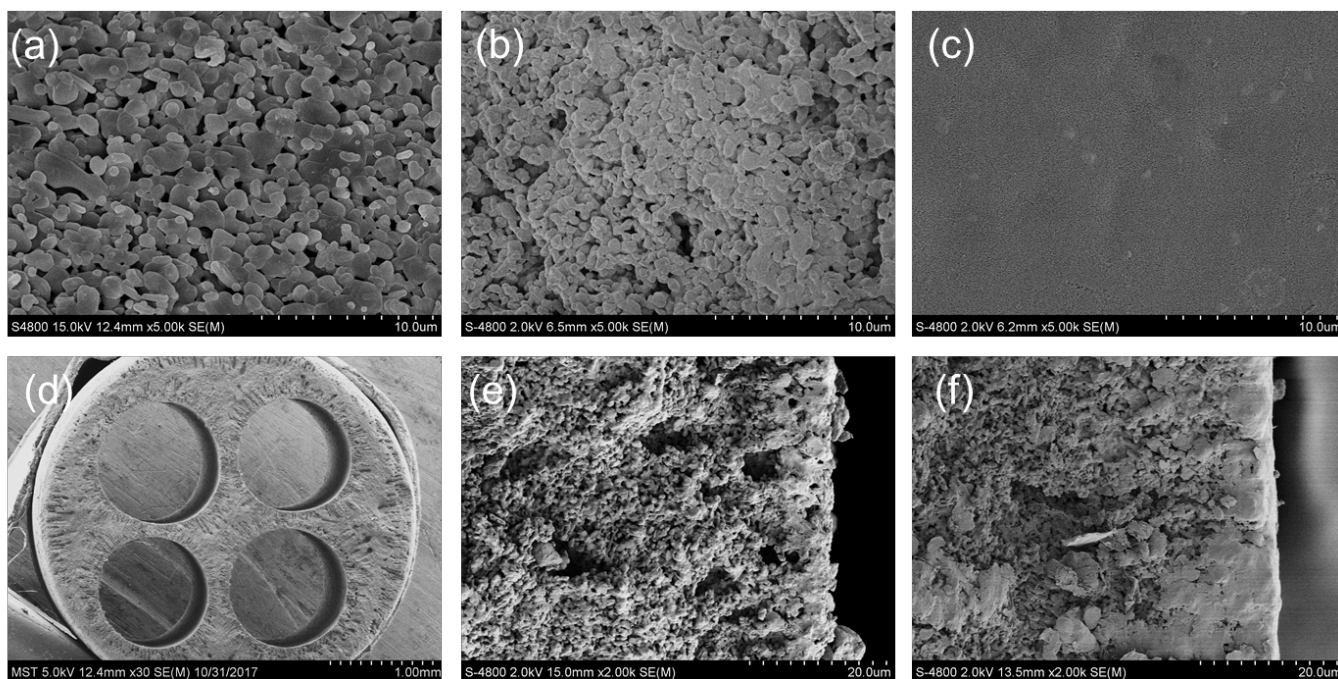


**Figure 12.** SEM images of 4-channel hollow fiber membranes: (a, d) support; (b, e)  $\text{TiO}_2$  membrane; (c, f)  $\text{TiO}_2\text{@MXene}$  (1 wt%). Surface: a-c; cross-section: d-f.

As expected, the pristine  $\text{TiO}_2$  hydrosols were almost filtrated through the hollow fiber support, resulting in a defective separation layer in the  $\text{TiO}_2$  membrane, as clearly indicated in Figures 12 (b, e). Effectively, by introducing 1 wt% MXene in the  $\text{TiO}_2$  hydrosols, a smooth and integrated membrane layer with a thickness of  $\sim 4\ \mu\text{m}$  was successfully formed on the hollow fiber support (Figures 12c&f). We further used EDX mapping to study the element distribution on the membrane surface. Al and Ti elements were selected to distinguish the alumina support from the  $\text{TiO}_2$  layer, and the typical results are shown in Figure 13. Very few Ti whereas large amounts of Al are detected in the surface of pristine  $\text{TiO}_2$  hollow fiber membrane, suggesting the uncovered alumina support caused by the significant sol infiltration into the macropores of the hollow fiber. In contrast, very strong Ti signals are detected in the surface of  $\text{TiO}_2\text{@MXene}$  membrane (1 wt%), along with very weak Al signals. The results agree well with the SEM image, again confirming that the sol infiltration was highly inhibited even if the substrates possessing larger pore size and run-through-macropores. These results verifies the methodology illustrated in Figure 1. The introduced 2D MXene nanosheets are believed to play a ‘floor tiles’-like role on the surface of the support and prevent the infiltration of the  $\text{TiO}_2$  NPs in the hydrosols. This smart design results in a reduced transport resistance and



leads to a highly integrated separation layer. It's particularly useful for the case of using large sized pores of support that presumably provides higher flux.

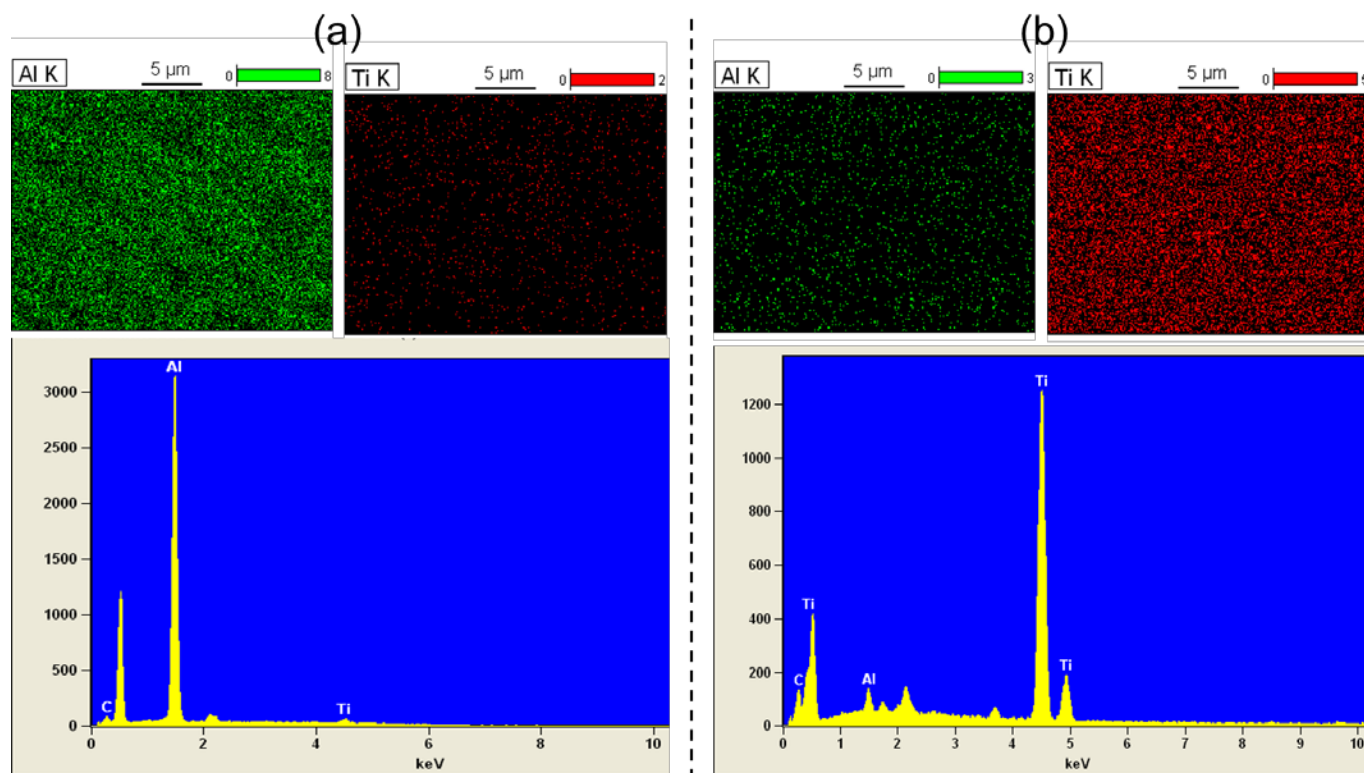


**Figure 13.** Surface EDX mapping of (a) TiO<sub>2</sub> and (b) TiO<sub>2</sub>@MXene (1 wt%) hollow fiber membranes

Filtration experiments are carried out to investigate the separation properties of the resulting hollow fiber membranes. Figure 14 shows the pure water flux, dextran retention and calculated pore size of three samples from the same batch of prepared TiO<sub>2</sub>@MXene (1 wt%) membranes. We found that the results of all the membrane samples are very close to each other, suggesting a good reproducibility of the TiO<sub>2</sub>@MXene hollow fiber membranes. Meanwhile, it's worth noting that these hollow fiber membranes possessed an excellent permeate flux of  $>90 \text{ L m}^2 \text{ h}^{-1} \text{ bar}^{-1}$ , and 90% MWCO of  $\sim 22,000 \text{ Da}$ . The flux is one order of magnitude higher than the disc membranes with better rejection characteristics. The smaller MWCO can be owing to the thicker TiO<sub>2</sub>@MXene layer on the hollow fiber support that may further eliminate pinhole defects. Importantly, the larger sized, more porous hollow fiber support exhibit much lower transport resistance and higher pure water flux of  $2200 \text{ L m}^2 \text{ h}^{-1} \text{ bar}^{-1}$ , enabling the high flux in the resulting TiO<sub>2</sub>@MXene hollow fiber membrane. As controls, the macroporous hollow fiber support and the defective

pristine  $\text{TiO}_2$  hollow fiber membrane were unable to show effective rejection of the dextran. The distinct filtration performance in the  $\text{TiO}_2$  hollow fiber membranes with or without introducing MXene, further highlighting the critical role of 2D MXene nanosheet in achieving high water flux and rejection via preventing the sol infiltration and promoting the formation of defect-free separation layer.

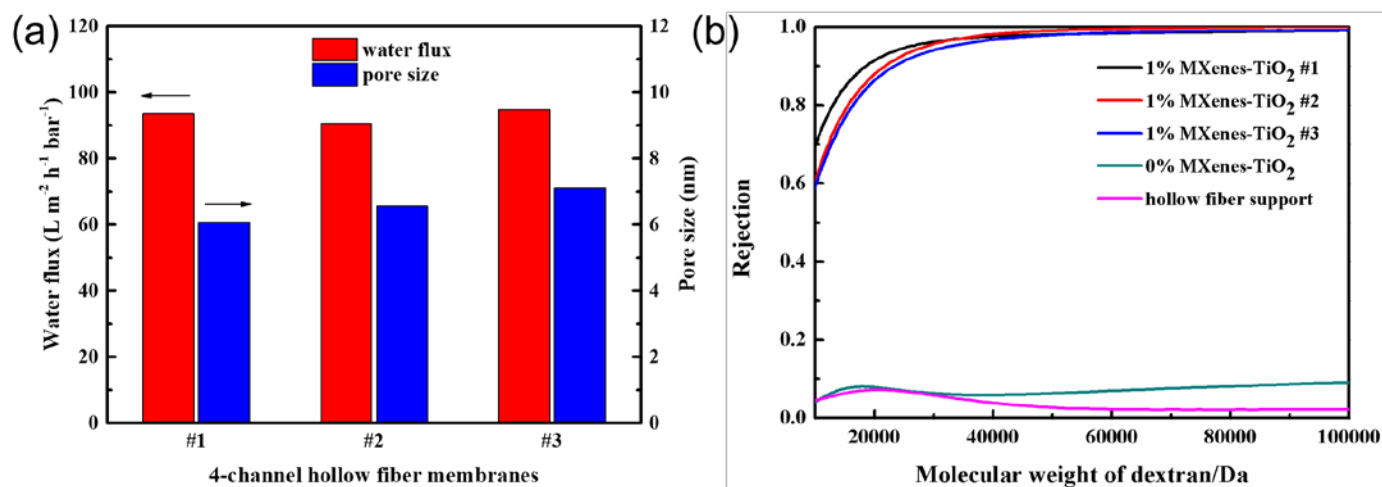


**Figure 14.** filtration performance of 4-channel hollow fiber membranes: (a) pure water flux and estimated pore size of three  $\text{TiO}_2$ @MXene (1 wt%) membrane samples; (b) dextran rejection of the support,  $\text{TiO}_2$  membrane and three  $\text{TiO}_2$ @MXene (1 wt%) membrane samples

## 4. Conclusions

In summary, this work demonstrated a simple and scalable synthetic method for developing high-quality mesoporous  $\text{TiO}_2$ @MXene membranes. Benefiting from the ‘floor title’ effect of the introduced 2D MXene nanosheets, the sol infiltration of  $\text{TiO}_2$  nanoparticles, which led to membrane defects and high transport resistance, was effectively inhibited. A crack-free  $\text{TiO}_2$ @MXene layer was successfully formed on macroporous discs by a single cycle of coating, aging, and calcination, which would significantly simplify the process and reduce the cost of membrane fabrication. Similarly, the  $\text{TiO}_2$ @MXene membranes were fabricated on the hollow fiber support via dip-coating. These hollow fibre membranes exhibited a high and reproduceable filtration performance, with pure water flux of  $>90 \text{ L m}^2 \text{h}^{-1} \text{bar}^{-1}$  and a cutoff molecular

weight of ~22,000 Da, showing great potential for practical application of these novel mesoporous membranes.

## Acknowledgments

This work is financially supported by the National Key Research and Development Program of China (2017YFB0306901), the National Natural Science Foundation of China (21676139), the Higher Education Natural Science Foundation of Jiangsu Province (15KJA530001), Research Fund of State Key Laboratory of Materials-Oriented Chemical Engineering (ZK201604) and the Project of Priority Academic Program Development of Jiangsu Higher Education Institutions (PAPD). Dr Xu is sponsored by China Regenerative Medicine International (CRMI) through a technology centre grant.

## Reference

- [1] M. Renzi, M. Agostini, M.A. Navarra, F. Nobili. An innovative membrane-electrode assembly for efficient and durable polymer electrolyte membrane fuel cell operations, *Int J Hydrogen Energ.* 42 (2017) 16686-16694.
- [2] J. Lu, L. Cheng, Y. Wang, Y. Ding, M. Hu, S. Li, Q. Zhai, Y. Jiang. Enzymatic-photocatalytic synergetic effect on the decolorization of dyes by single chloroperoxidase molecule immobilization on TiO<sub>2</sub> mesoporous thin film, *Materater Design.* 129 (2017) 219-226.
- [3] R. Chen, X. Cheng, X. Zhu, Q. Liao, L. An, D. Ye, X. He, Z. Wang. High-performance optofluidic membrane microreactor with a mesoporous CdS/TiO<sub>2</sub> /SBA-15@carbon paper composite membrane for the CO<sub>2</sub> photoreduction, *Chem Eng J.* 316 (2017) 911-918.
- [4] L. Yan, D. Li, S. Li, Z. Xu, J. Dong, W. Jing ; W. Xing. Balancing Osmotic Pressure of Electrolytes for Nanoporous Membrane Vanadium Redox Flow Battery with a Draw Solute, *ACS Appl. Mater. Inter.* 8 (51) (2016) 35289-35297
- [5] D. Li, W. Jing , S. Li, H. Shen, W. Xing. Electric Field-Controlled Ion Transport In TiO<sub>2</sub> Nanochannel, *ACS Appl. Mater. Inter.* 7 (2015) 11294-11300.

- [6] X. Cao, W. Jing, W. Xing, Y. Fan, Y. Kong, J. Dong. Fabrication of a visible-light response mesoporous TiO<sub>2</sub> membrane with superior water permeability via a weak alkaline sol-gel process, *Chem Commun (Camb)*. 47 (2011) 3457-3459.
- [7] W. Jing, W. Huang, W. Xing, Y. Wang, W. Jin, Y. Fan. Fabrication of Supported Mesoporous TiO<sub>2</sub> Membranes: Matching the Assembled and Interparticle Pores for an Improved Ultrafiltration Performance, *ACS Appl. Mater. Inter.* 1 (2009) 1607-1612.
- [8] Z. Dong, W. Jing, W. Xing. Triblock polymer template assisted sol-gel process for fabrication of multi-channel TiO<sub>2</sub>/ZrO<sub>2</sub> ultrafiltration membrane, *J. Membr. Sci.* 373 (2011) 167-172.
- [9] D. Zou, M. Qiu, X. Chen, Y. Fan, One-step preparation of high-performance bilayer  $\alpha$ -alumina ultrafiltration membranes via co-sintering, *J. Membr. Sci.* 524 (2017) 141-150.
- [10] D. Li, H. Wang, W. Jing, Y. Fan, W. Xing. Fabrication of mesoporous TiO<sub>2</sub> membranes by a nanoparticle-modified polymeric sol process, *J. Colloid Interface Sci.* 433 (2014) 43-48.
- [11] Y. Cai, Y. Wang, X. Chen, M. Qiu, Y. Fan. Modified colloidal sol-gel process for fabrication of titania nanofiltration membranes with organic additives, *J. Membr. Sci.* 476 (2015) 432-441.
- [12] Y. Yin, H. Wang, D. Li, W. Jing, Y. Fan, W. Xing. Fabrication of mesoporous titania-zirconia composite membranes based on nanoparticles improved hydrosol, *J. Colloid Interface Sci.* 478 (2016) 136-144.
- [13] K. Huang, G. Liu, Y. Lou, Z. Dong, J. Shen, W. Jin. A Graphene Oxide Membrane with Highly Selective Molecular Separation of Aqueous Organic Solution, *Angewandte Chemie International Edition*. 53 (2014) 6929-6932.
- [14] J. Shen, G. Liu, K. Huang, W. Jin, K. Lee, N. Xu. Membranes with Fast and Selective Gas-Transport Channels of Laminar Graphene Oxide for Efficient CO<sub>2</sub> Capture, *Angew. Chem., Int. Ed.* 54 (2014) 578-582.
- [15] R.K. Joshi, P. Carbone, F.C. Wang, V.G. Kravets, Y. Su, I.V. Grigorieva, H.A. Wu, A.K. Geim, R.R. Nair. Precise and Ultrafast Molecular Sieving Through Graphene Oxide Membranes, *Science*. 343 (2014) 752-754.
- [16] Y.L.Y.B. Y. Peng. Metal-organic framework nanosheets as building blocks for molecular sieving membranes, *Science*. 346 (2014) 1135-1356.

- [17] K. Varoon, X. Zhang, B. Elyassi, D.D. Brewer, M. Gettel, S. Kumar, J.A. Lee, S. Maheshwari, A. Mittal, C.Y. Sung, M. Cococcioni, L.F. Francis, A.V. McCormick, K.A. Mkhoyan, M. Tsapatsis. Dispersible Exfoliated Zeolite Nanosheets and Their Application as a Selective Membrane, *Science*. 334 (2011) 72-75.
- [18] G. Liu, W. Jin, N. Xu, Two  
Membranes, *Angew. Chem., Int. Ed.* 55 (2016) 13384-13397
- [19] M. Naguib, O. Mashtalir, J. Carle, V. Presser, J. Lu, L. Hultman, Y. Gogotsi, M.W. Barsoum. Two-Dimensional Transition Metal Carbides. *ACS NANO*. 6 (2012) 1322-1331.
- [20] M. Naguib, M. Kurtoglu, V. Presser, J. Lu, J. Niu, M. Heon, L. Hultman, Y. Gogotsi, M.W. Barsoum. Two-Dimensional Nanocrystals Produced by Exfoliation of  $\text{Ti}_3\text{AlC}_2$ , *Adv. Mater.* 23 (2011) 4248-4253.
- [21] O.M.C.E. M. R. Lukatskaya. Cation Intercalation and High Volumetric Capacitance of Two-Dimensional Titanium Carbide, *Science*. 341 (2013) 1502-1505.
- [22] M. Naguib, J. Halim, J. Lu, K.M. Cook, L. Hultman, Y. Gogotsi, M.W. Barsoum. New Two-Dimensional Niobium and Vanadium Carbides as Promising Materials for Li-Ion Batteries, *J. Am. Chem. Soc.* 135 (2013) 15966-15969.
- [23] T.Y. Ma, J. Ran, S. Dai, M. Jaroniec, S.Z. Qiao. Phosphorus-Doped Graphitic Carbon Nitrides Grown In Situ on Carbon-Fiber Paper: Flexible and Reversible Oxygen Electrodes, *Angew. Chem., Int. Ed.* 54 (2015) 4646-4650.
- [24] Y. Ying, Y. Liu, X. Wang, Y. Mao, W. Cao, P. Hu, X. Peng. Two-Dimensional Titanium Carbide for Efficiently Reductive Removal of Highly Toxic Chromium(VI) from Water, *ACS Appl. Mater. Inter.* 7 (2015) 1795-1803.
- [25] J.G.Q.Z. Q. Peng. Unique Lead Adsorption Behavior of Activated Hydroxyl Group in, *J. Am. Chem. Soc.* 136 (2014) 4113-4116.
- [26] Y.T.C.Y. JianFeng Zhu. Composites of  $\text{TiO}_2$  Nanoparticles Deposited on  $\text{Ti}_3\text{C}_2$  MXene Nanosheets with Enhanced Electrochemical Performance, *J. Electrochem. Soc.* 163 (2016) A785-A791.
- [27] C.E. Ren, K.B. Hatzell, M. Alhabeb, Z. Ling, K.A. Mahmoud, Y. Gogotsi, Charge- and Size-Selective Ion Sieving Through  $\text{Ti}_3\text{C}_2\text{T}_x$  MXene Membranes, *J. Phys. Chem. Lett.* 6 (2015) 4026-4031;
- [28] L. Chen, G. Shi, J. Shen, B. Peng, B. Zhang, Y. Wang, F. Bian, J. Wang, D. Li, Z. Qian, G. Xu, G. Liu, J. Zeng, L. Zhang, Y. Yang, G. Zhou, M. Wu, W. Jin, J. Li, H. Fang, Ion sieving in graphene oxide membranes via cationic control of interlayer spacing, *Nature*. doi:10.1038/nature24044

-Dimens

- [29] A. Huang, Q. Liu, N. Wang, Y. Zhu, J. Caro, Bicontinuous Zeolitic Imidazolate Framework ZIF-8@GO Membrane with Enhanced Hydrogen Selectivity, *J. Am. Chem. Soc.* 136 (2014) 14686-14689;
- [30] Y. Hu, J. Wei, Y. Liang, H. Zhang, X. Zhang, W. Shen, H. Wang, Zeolitic Imidazolate Framework/Graphene Oxide Hybrid Nanosheets as Seeds for the Growth of Ultrathin Molecular Sieving Membranes, *Angew. Chem., Int. Ed.* 55 (2016) 2048-2052;
- [31] Zhang, M., Guan, K., Shen, J., Liu, G., Fan, Y. and Jin, W. Nanoparticles@rGO membrane enabling highly enhanced water permeability and structural stability with preserved selectivity, *AIChE J.* 63 (2017) 5054–5063
- [32] S. Liu, K. Li, R. Hughes. Preparation of porous aluminium oxide ( $\text{Al}_2\text{O}_3$ ) hollow fibre membranes by a combined phase-inversion and sintering method, *Ceram. Int.* 29 (2003) 875–881.
- [33] C. Cai, Y. Zhang, C. Zhang and X. Gu, Microstructure modulation of  $\alpha$  ~~204~~ hollow fiber membranes with four ~~channels~~ ~~Chem Eng Commun~~ ~~2016~~ ~~249~~ ~~457~~.
- [34] A. Lipatov, M. Alhabeb, M.R. Lukatskaya, A. Boson, Y. Gogotsi, A. Sinitskii, Effect of Synthesis on Quality, Electronic Properties and Environmental Stability of Individual Monolayer  $\text{Ti}_3\text{C}_2$  MXene Flakes, *Advanced Electronic Materials*, 2 (2016) 1600255.
- [35] C.J. Zhang, S. Pinilla, N. McEvoy, C.P. Cullen, B. Anasori, E. Long, S.-H. Park, A. Seral-Ascaso, A. Shmeliov, D. Krishnan, C. Morant, X. Liu, G.S. Duesberg, Y. Gogotsi, V. Nicolosi, Oxidation Stability of Colloidal Two-Dimensional Titanium Carbides (MXenes), *Chemistry of Materials*, 29 (2017) 4848-4856.